PHYSICAL REVIEW E VOLUME 54, NUMBER 5 NOVEMBER 1996

Temporal modulation of traveling waves in the flow between rotating cylinders with broken azimuthal symmetry

Sarath G. K. Tennakoon* and C. David Andereck
Department of Physics, The Ohio State University, 174 West 18th Avenue, Columbus, Ohio 43210

John J. Hegseth
Department of Physics, University of New Orleans, New Orleans, Louisiana 70148

Hermann Riecke
Department of Engineering Sciences and Applied Mathematics, Northwestern University, Evanston, Illinois 60208

(Received 8 April 1996)

The effect of temporal modulation on traveling waves in the flows in two distinct systems of rotating cylinders, both with broken azimuthal symmetry, has been investigated. It is shown that by modulating the control parameter at twice the critical frequency one can excite phase-locked standing waves and standing-wave-like states that are not allowed when the system is rotationally symmetric. We also show how previous theoretical results can be extended to handle patterns such as these, which are periodic in two spatial directions. [S1063-651X(96)04711-3]

PACS number(s): 47.20.−k, 47.27.Ak

I. INTRODUCTION

The behavior of pattern forming systems under external time-periodic forcing has been the subject of intense investigation over the past several years [1,2]. Since such periodically forced flows are common in nature and technological applications [3], a knowledge of their stability properties may have important practical applications.

There have been several experimental and theoretical studies investigating the effect of time-periodic forcing on the stability of the axisymmetric *steady* spatial patterns produced in the flow between two rotating cylinders (Taylor-Couette flow) [4–10]. These studies found that temporal modulation of control parameters can stabilize or destabilize the primary flows; the spatial properties of the base flow and the axisymmetric Taylor vortex flow remain, however, largely unaffected by the modulation. Only a very small shift of the instabilities in the parameter space has been observed in these systems.

For wave structures, however, recent studies by Riecke, Crawford, and Knobloch [11] and Walgraef [12] have shown that for the appropriate frequency of an external forcing a strong resonance may occur between the forcing and the spatiotemporal patterns. This can transform initially stable traveling waves into standing waves or quasiperiodic structures. This kind of behavior has been experimentally observed in electroconvection of nematic liquid crystals and in binary fluid convection by Rehberg *et al.* [13]. It is also related to the parametric excitation of surface waves (Faraday waves) [14].

In this paper we investigate the effect of temporal modulation on the traveling-wave patterns that appear near the primary bifurcation boundary of two rotating cylinder systems with broken rotational symmetry. First, we will discuss the theoretical background for this study. Next, we will describe our experimental studies of the modulated *Taylor-Dean* and *Taylor-Couette* systems. Finally, we will compare the experimental observations with the theoretical predictions.

II. THEORY

Using symmetry arguments and suitable amplitude equations it has been shown previously [11,12,15] that a resonant temporal forcing can excite standing waves in an effectively one-dimensional extended system undergoing a Hopf bifurcation to traveling waves. Here we will extend those arguments to systems that are periodic in two directions. This is necessary for spiral vortex flow since the azimuthal symmetry of the concentric Taylor system imposes additional constraints on the amplitude equations.

The excitation of standing waves by resonant forcing can be understood intuitively by an extension of the standard example of a parametrically forced pendulum. In that case, a periodic parametric forcing such as, e.g., the periodic variation of the length of the pendulum, leads to a periodic pumping of energy into and out of the pendulum. In order to effect a net increase in the pendulum's energy the pumping and the pendulum have to have a certain phase relationship; in particular, the frequencies have to be resonant. Maximal efficiency is achieved if the forcing frequency is twice the natural frequency of the pendulum (e.g., decreasing the length of the pendulum whenever it travels downward).

Considering extended systems as an array of coupled pendulums makes it clear that only standing waves, but not traveling waves, can be excited parametrically: in a standing wave all oscillators have the same phase (albeit different amplitudes) and therefore all of them can satisfy the phase relationship necessary for excitation simultaneously; in a traveling wave the phases are distributed evenly over the

---

*Present address: Department of Physics, Duke University, Box 90305, Durham, NC 27708.

circle and the out-of-phase oscillators will lose the energy gained by the in-phase oscillators.

To consider spiral vortex flow, which arises in a fluid between counterrotating concentric cylinders [16], one has to extend this consideration to two dimensions since the spirals are periodic along the axis *and* along the azimuthal direction. Therefore, the superposition of oppositely traveling spirals (''ribbons'') leads to waves that are standing in the axial direction but traveling in the azimuthal direction. Thus the periodic forcing may pump energy into the ribbon at some azimuthal angle, but will extract energy at the same time at a different angle. For a net increase these energies have to be different, which is achieved by an azimuthally dependent perturbation of the forcing. Alternatively, the azimuthal symmetry of the system itself can be broken. Maximal efficiency is achieved, in analogy to the temporal forcing, if the azimuthal wave number of the perturbation is twice the azimuthal wave number of the ribbon.

The above arguments can be made precise by considering spiral vortex flow near its onset where its amplitude is small. Then the periodic forcing as well as the azimuthal perturbation can also be taken small and the system can be described by coupled amplitude equations. The crucial ingredients are the critical eigenvectors of the system, i.e., those modes that have small (or zero) growth rate, since they define the center manifold of the system in this parameter regime. In the present case the critical modes are the two spiral wave modes of the flow field $\mathbf{v}$ as well as the periodic forcing F and the azimuthal perturbation P,

$$\mathbf{v}=A(T)e^{iqz+i\omega_ht+im\phi}\mathbf{f}_a(r)+B(T)e^{iqz-i\omega_ht-im\phi}\mathbf{f}_b(r)+\text{c.c.}+(\text{higher-order terms}), \tag{1}$$

$$F=be^{i\omega_et}+\text{c.c.}, \tag{2}$$

$$P=we^{in\phi}+\text{c.c.} \tag{3}$$

Here T is a slow time and $\mathbf{f}_{a,b}(r)$ are the radial eigenvectors of the spiral vortex flow. The axis of the cylinders is taken along the z direction and ϕ is the azimuthal angle. The frequencies ω_h and ω_e are the Hopf frequency of the spirals and the frequency of the forcing, respectively. Below we will choose ω_e close to $2\omega_h$. The difference will determine the detuning. Although the forcing and the azimuthal perturbation are imposed externally we consider them as dynamical variables and include them in the center manifold. This simplifies the derivation of the relevant amplitude equations for $A(T)$ and $B(T)$. Their form is obtained by considering the most general polynomial that is consistent with the symmetries of the system (in the absence of forcing $F=0$ and the azimuthal perturbation $P=0$): translation symmetry in space along z, rotational symmetry in ϕ, translational symmetry in time t, and reflection symmetry in z. These symmetries allow a linear coupling of the left and right spiral amplitudes via the forcing and azimuthal perturbation only if the frequencies ω_e and ω_h as well as the azimuthal wave numbers m and n are related as

$$\frac{2\omega_h}{\omega_e}=k, \quad \frac{2m}{n}=l, \quad k,l=1,2,3,\ldots\,. \tag{4}$$

Simply put, under these conditions the term $Bb^kw^le^{iqz-i\omega_ht-im\phi}e^{ik\omega_et}e^{iln\phi}$ corresponds to the same Fourier coefficient in z, t, and ϕ as $Ae^{iqz+i\omega_ht+im\phi}$ and can therefore arise in the evolution equation for A, thus providing the crucial *linear* coupling. To cubic order one then obtains the equations

$$\partial_TA=aA+db^kw^{2m/n}B+c|A|^2A+g|B|^2A, \tag{5}$$

$$\partial_TB=a^*B+db^kw^{2m/n}A+c^*|B|^2B+g^*|A|^2B, \tag{6}$$

$$\partial_Tb=0, \quad \partial_Tw=0. \tag{7}$$

The real part a_r of the coefficient a gives the growth rate of the spiral waves and is proportional to the distance from the Hopf bifurcation. Thus $a_r=\alpha(R_i-R_{ic})$, with R_i the Reynolds number for the inner cylinder and R_{ic} its critical value. To allow for a small detuning in the forcing, the frequency ω_h in (1) is replaced by $\omega_e/2$. The detuning ξ is then related to the imaginary part a_i as

$$\xi\equiv\frac{\omega_h-\omega_e/2}{\omega_h}=\frac{a_i-\gamma a_r}{\omega_h}, \tag{8}$$

where the term γa_r accounts for the change of the linear frequency with the control parameter R_i. The coefficients d, c, and g are in general complex, whereas the product $db^kw^{2m/n}$ can be chosen real. All coefficients are functions of the invariants $|b|^2$ and $|w|^2$. This is most relevant for the small coefficient a. Thus the forcing and the azimuthal perturbation lead to a shift in the threshold and of the Hopf frequency even in the nonresonant case.

Equations (5) and (6) show that the forcing and the azimuthal perturbation have a maximal effect if $k=1$ and $l\equiv 2m/n=1$, i.e., if the external frequency is twice the Hopf frequency and the wave number of the azimuthal perturbation is twice that of the spiral waves. Unfortunately, the latter condition cannot be implemented easily in the Taylor-Couette experiments since eccentrically mounted cylinders yield a perturbation of the form $\cos\phi$, i.e., $n=1$. The eccentricity leads therefore to a term in the amplitude equations that is only of order $w^{2m}\ll w$ (for $m\geqslant 1$). It is worth noting that even if the azimuthal perturbation was not a pure $\cos\phi$, but contained also its harmonics, $P=\Sigma_{r=-\infty}^{\infty}w_r\exp(ir\phi)$, the lowest-order term (in A and B) breaking the time-translation symmetry would still be as given in (5) and (6), with $w^{2m/n}$ replaced by a more general function reflecting the contributions from the various harmonics. This function could be written as a sum of products $w_{r^{(1)}}w_{r^{(2)}}w_{r^{(3)}}\cdots$ with $r^{(1)}+r^{(2)}+r^{(3)}+\cdots=2m$. If present, the harmonic with wave number $r=2m$ would be dominant in the limit of small azimuthal perturbation since it enters with the lowest power. For the experiments presented in this paper the main observation is that *in the absence of any azimuthal perturbations* $(w=0)$ *no linear coupling of oppositely traveling waves occurs and the standing waves in question cannot arise directly from the basic state* $A=0=B$ *through a linear instability*.

The amplitude equations (5) and (6) have been analyzed previously in detail [11,12] for the case $g_r<c_r<0$, i.e., for a Hopf bifurcation to stable traveling waves rather than (unlocked) standing waves. The main result is the excitation of standing waves, $|A|=|B|=$const, by the periodic forcing be-

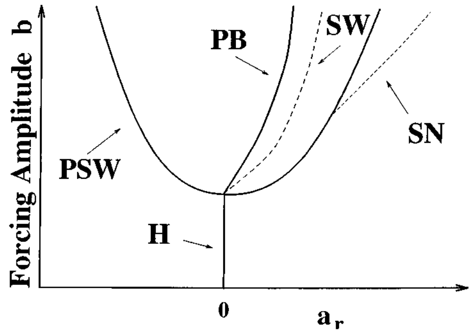

FIG. 1. Sketch of a typical phase diagram for modulated rotation at resonance ($\omega_e = 2\omega_h$), where the loci of various transitions are given as a function of the forcing strength (measured by b) and mean Reynolds number (measured by a_r). The transition from the basic state to standing waves occurs along the line marked PSW and from the basic state to traveling waves occurs along the line marked H.

low the Hopf bifurcation ($a_r < 0$). As it is clear from the fact that the amplitudes A and B are constant in time, these waves are phase locked to the forcing [cf. (1) with $\omega_h \to \omega_e/2$]. A sketch of a typical phase diagram is shown in Fig. 1, where the loci of various transitions are given as functions of the forcing strength (measured by b) and the mean Reynolds number (measured by a_r). The transition from the basic state of purely azimuthal flow to the phase-locked standing waves (ribbons) occurs along the line marked PSW, which is given by

$$b^2 = \frac{a_r^2 + a_i^2}{(dw^{2m/n})^2} = \frac{a_r^2 + (\xi\omega_h + \gamma a_r)^2}{(dw^{2m/n})^2}. \tag{9}$$

Along the line marked H the basic state undergoes a Hopf bifurcation to traveling waves as well as (unstable) standing waves. This bifurcation exists already in the absence of any periodic forcing ($b = 0$). Along the line marked PB the phase-locked standing waves become unstable to the traveling waves in a secondary parity-breaking bifurcation. Not relevant for this experiment are the transition of the unstable phase-locked standing waves to unstable standing waves at SW and the saddle-node bifurcation of the phase-locked standing waves along SN.

To obtain quantitative results pertaining to spiral vortex flow the linear as well as the nonlinear coefficients have to be determined numerically. This is a formidable task and will not be attempted here. It should be noted, however, that to leading order the nonlinear coefficients c and g are not affected by the forcing and the azimuthal perturbation. Thus the values for the concentric case can be used, which have been determined previously [17].

In addition to the results on modulated spirals in the slightly eccentric Taylor system, we will also present results on traveling inclined rolls, which occur in the Taylor-Dean system [18]. In this system the azimuthal symmetry is broken strongly. Therefore, instead of the discussion presented above the original derivation of the amplitude equations in the presence of a single translation symmetry applies [11,12,15]. It is based on an expansion of the flow field in the form

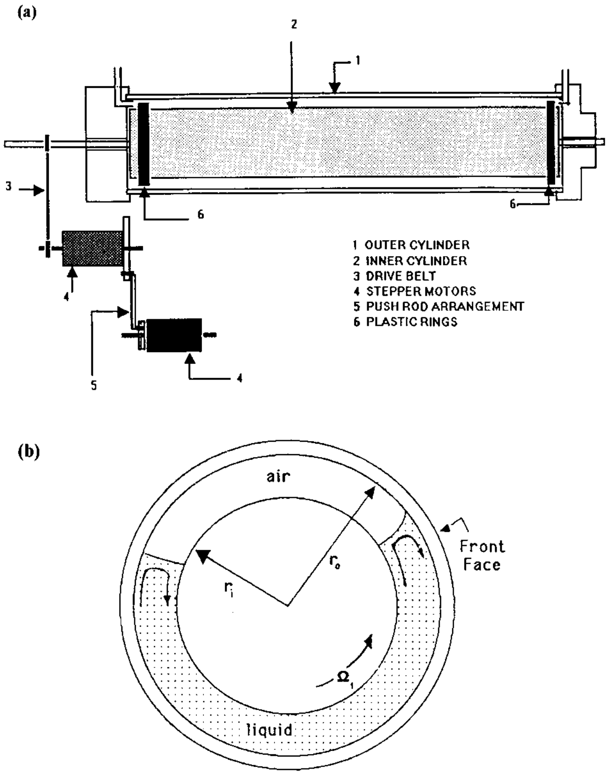

FIG. 2. (a) Schematic diagram of the Taylor-Dean apparatus. (b) Schematic cross section of the apparatus. The front side is the side where the observer sees the inner cylinder rotating upward as shown.

$$\mathbf{v} = A(T)e^{iqz + i\omega_h t}\mathbf{f}_a(r,\phi) + B(T)e^{iqz - i\omega_h t}\mathbf{f}_b(r,\phi) + \text{c.c.} + (\text{higher-order terms}) \tag{10}$$

and leads to (5) and (6) with $w = 1$.

III. EXPERIMENTAL APPARATUS AND PROCEDURES

Two variations of the concentric rotating cylinder (Taylor-Couette) system were employed to test the concepts of Sec. II. The systems break the rotational symmetry in very different ways. In the next few sections, we will describe each one in detail. First, we present the experimental system with strongly broken rotational symmetry, the Taylor-Dean system.

A. Taylor-Dean system

The Taylor-Dean system consists of two independently rotating horizontal coaxial cylinders with a partially filled gap (see Fig. 2) [18,19]. The partial filling of the gap in the Taylor-Dean system breaks the rotational symmetry of the flow. The rotation of the cylinders and the two free surfaces impose a pressure gradient along the azimuthal direction. As a result, the flow sufficiently far away from the free surfaces is a combination of Couette flow due to rotation of the cylinders and Poiseuille flow due to the azimuthal pressure gradient. The main control parameters of this system are the inner and outer cylinder Reynolds numbers $R_i = 2\pi f_i r_i d/\nu$ and $R_o = 2\pi f_o r_o d/\nu$, where f_o and f_i are the outer and inner

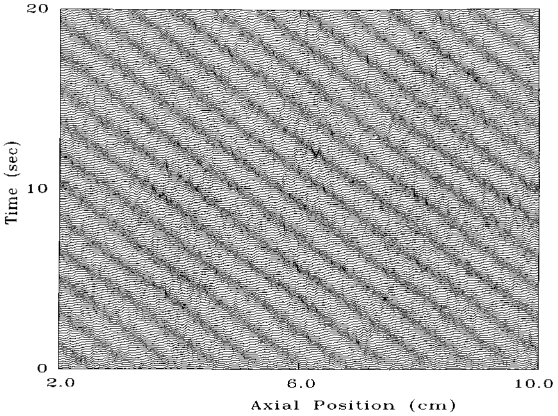

FIG. 3. Space-time diagram of the traveling roll pattern in the Taylor-Dean system when $R_i=265$, $R_o=0$, and $R_m=0$. The wavelength of the pattern is $\lambda=0.841$ cm and the frequency is 0.543 Hz.

cylinders' rotational frequencies, d is the gap width, and ν is the kinematic viscosity of the fluid. As the control parameters are varied the base flow instabilities change from those associated with Taylor-Couette to those associated with Dean flow. An initial experimental work with the Taylor-Dean system was done by Brewster and Nissan [20], who studied the threshold of the instability when the inner cylinder rotates and the outer cylinder is stationary. More recently, Mutabazi, Normand, Peerhossaini, and Wesfreid [21] have solved the linear stability problem for axisymmetric and nonaxisymmetric perturbations in the flow. They found both stationary- and traveling-wave instabilities depending on the ratio of the angular velocities μ $(=f_o/f_i)$ [19]. We kept the outer cylinder stationary $(R_o=0)$ for this study, while rotating the inner cylinder. In this case the first transition from the unperturbed base flow is to traveling inclined rolls as the inner cylinder speed increases, as shown in the experimental study of Mutabazi, Hegseth, Andereck, and Wesfreid [18]. The transition to traveling inclined rolls is, within the experimental error, a supercritical Hopf bifurcation. At onset these rolls also have no preferred direction and may move either left or right along the cylinder axis. Therefore, this system can be used to verify the theoretical prediction that a breaking of the time translational symmetry by a small periodic modulation of the control parameter will result in a stable standing-wave pattern [11,12].

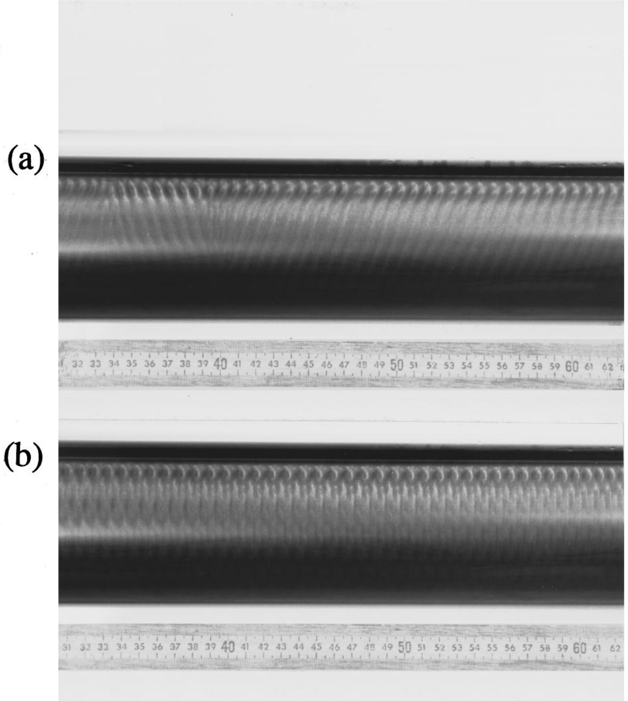

FIG. 4. Pictures of the (a) traveling roll (for $R_i=269$ and $R_m=0$) and (b) standing wave states in the Taylor-Dean system (for $R_i=265$ and $R_m/R_{ic}=0.28$).

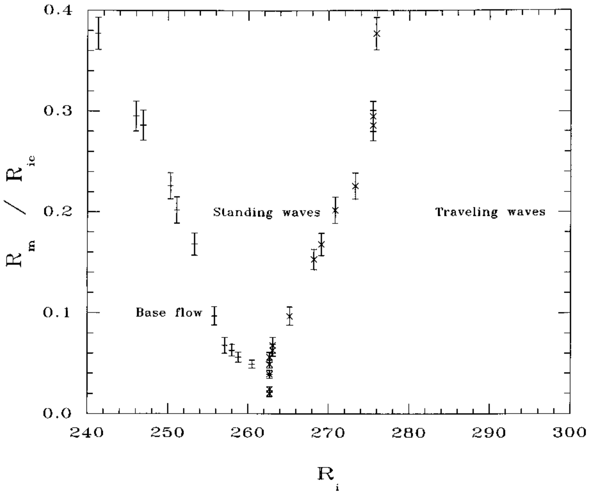

FIG. 5. Phase diagram of standing-wave and traveling-wave states of the Taylor-Dean system when the detuning parameter is $\xi=0$. The pluses and crosses indicate the location of the bifurcation from the base state to standing waves and standing waves to traveling waves, respectively.

Our experimental system consists of an inner cylinder made of black Delrin plastic with radius $r_i=4.47$ cm and a stationary outer cylinder made of Duran glass with radius $r_o=5.08$ cm, giving a gap $d=r_o-r_i=0.59$ cm and radius ratio $\eta=r_i/r_o=0.883$. Two plastic rings are attached to the inner cylinder a distance $L=52.4$ cm apart, giving an aspect ratio $\Gamma=L/d=88$, large enough to conceive of this as an extended system where one can neglect end effects. In this

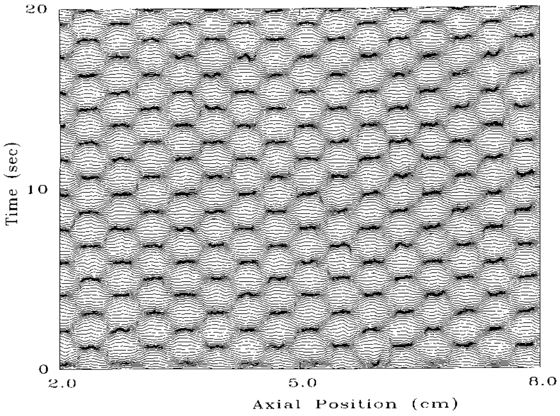

FIG. 6. Space-time diagram of the standing wave state at $R_m/R_i=0.30$, $R_i=241$, and $\xi=0\pm0.01$ (Taylor-Dean system).

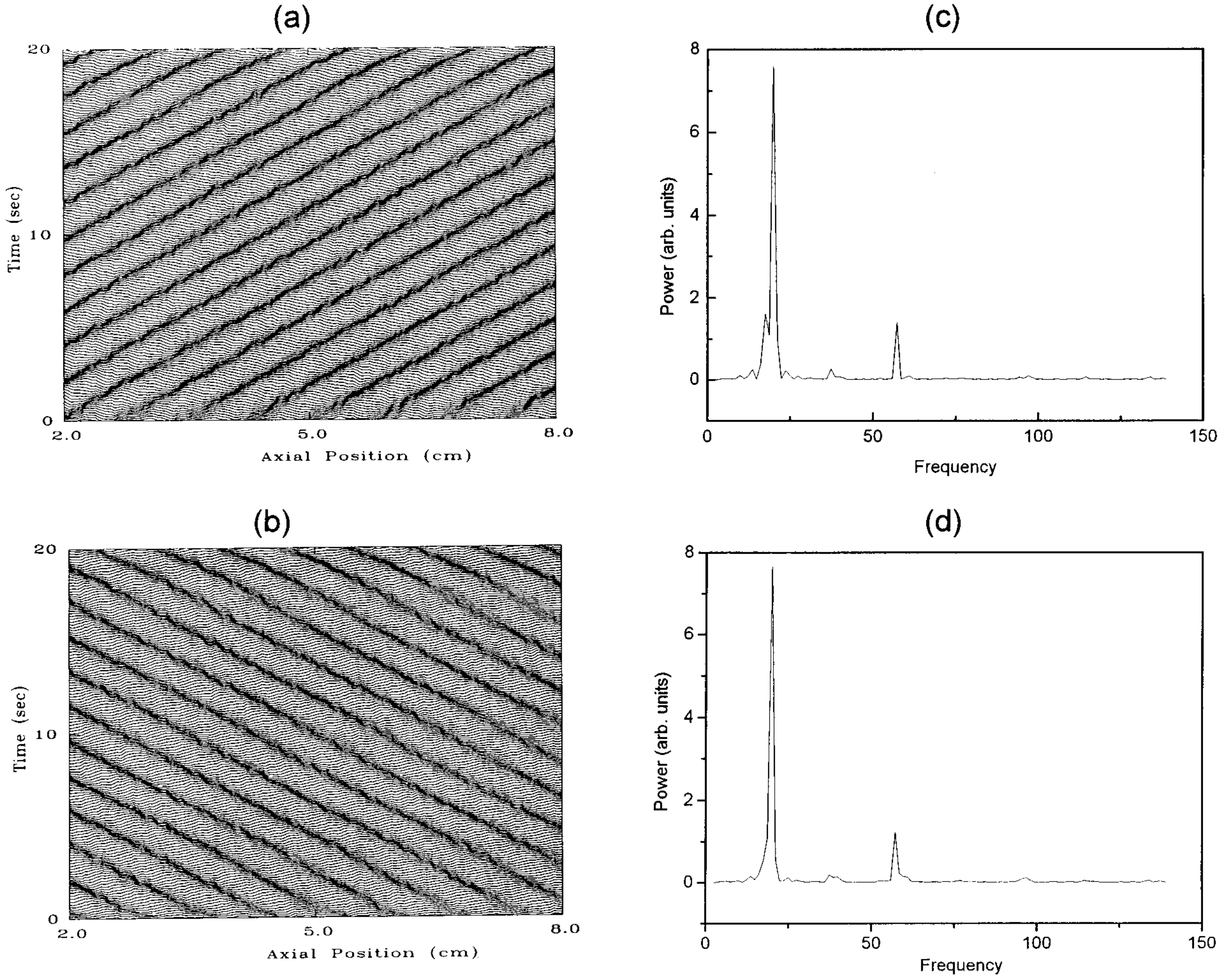

FIG. 7. Space-time diagrams of (a) the right-traveling-wave component and (b) the left-traveling-wave component of the standing-wave state shown in Fig. 6, obtained using a two-dimensional FFT decomposition. (c) and (d) are the frequency power spectra of the decomposed right- and left-traveling modes. The dimensionless frequencies are scaled to the inverse of the diffusive time scale ν/d^2.

system the filling level fraction $n=\theta_f/2\pi$ has been fixed at 0.75, where θ_f is the filling angle.

The working fluid was pure double distilled water or a solution of double distilled water and 44% glycerol by weight with 1% of Kalliroscope AQ1000 added for visualization. These nearly two-dimensional ($\approx 30\ \mu\text{m}\times 6\ \mu\text{m}\times 0.07\ \mu\text{m}$) polymeric flakes align along the streamline surfaces, reflecting light according to their orientation. Generally the dark areas indicate flow along the observer's line of sight, while the light areas indicate flow perpendicular to the line of sight. The apparatus was kept in a temperature controlled room so that the temperature of the working fluid was held constant to within 0.1 °C.

Spatial and temporal properties of the flow patterns were obtained using a 512×480 pixel charge coupled device (CCD) camera connected to an image processor. The image processor board, installed in a personal computer, captured a picture of the flow pattern and then a software routine was used to obtain the intensity along a single line parallel to the axis of the cylinders. This system is able to process up to one line every 0.11 sec. The data were then transferred to a VAX 4000-90 computer system and an analysis of the resulting intensity versus axial position as a function of time plots (space-time data plots) yields the wavelengths and the dynamics of the patterns in time and space.

In the Taylor-Dean system, we have used a combination of two stepper motors (Compumotor A83-93) to drive the inner cylinder, one motor to produce a net rotation and the other to produce a sinusoidal modulation of the inner cylinder angular velocity. The first motor was directly connected to the inner cylinder and rotated with constant angular velocity. The housing of this motor was oscillated by a push-rod arrangement mechanically coupled to the second motor (see Fig. 2). The rotation of the second motor gave a net output at the inner cylinder of a constant angular velocity plus a periodic sinusoidal variation in angular velocity.

The motor speeds were controlled through Compumotor 2100 Series indexers and could be changed either manually or through computer control. The motor speeds have a frequency accuracy of 0.02%. Typically, a computer controlled the rotation speed, direction, and ramping rates. Because both the frequency and amplitude of the modulation could be varied, this introduced two new control parameters into the system, as required by the theory.

The Reynolds number of the inner cylinder is now $R=R_i+R_m\sin(2\pi f_m t)$, where $R_m=2\pi f_a r_i d/\nu$ and f_a is the amplitude of the sinusoidal rotational frequency. The two dimensionless parameters are R_m/R_{ic} and the detuning parameter $\xi=(2f_h-f_m)/2f_h$, where R_{ic} is the critical Reynolds number for onset of the traveling roll pattern and f_h is the frequency of the traveling rolls (Hopf frequency) in the absence of modulation.

To obtain the location of the onset of patterns for each modulation frequency f_m and modulation amplitude R_m, we employed the following method. We first set the R_i value below the onset of instabilities and then increased it quasistatically (keeping both amplitude R_m and frequency f_m of modulation at a fixed value) until a flow pattern appeared in the system. Then several sets of space-time data were taken while increasing R_i. We repeated this procedure with increasing amplitudes and various frequencies around twice the Hopf frequency (the frequency of the traveling rolls near onset when there is no modulation).

B. Results and discussion

When there is no modulation ($R_m=0$), the base flow bifurcates supercritically to a traveling roll pattern as we increase the inner cylinder speed. A typical space-time diagram for the traveling roll pattern near onset ($R_i=265$, $R_o=0$, and $R_m=0$) is shown in Fig. 3. The wavelength of the rolls along the cylinders is $\lambda=0.841$ cm. At ϵ $[=(R_i-R_{ic})/R_{ic}]$ slightly greater than 0.0 the pattern fills most of the working space and both left- and right-traveling rolls may exist with a vertical defect line between them [see Fig. 4(a)]. The frequency of the traveling rolls (Hopf frequency) near the onset ($R_{ic}=263$) is 0.543 Hz. Upon further increase of R_i, the flow undergoes a second instability to a short-wavelength modulation of the traveling rolls at $R_i=303$ and then to an incoherent pattern at about $R_i=338$ [22].

The transition sequence changes dramatically with modulation of the inner cylinder speed. When we modulated the inner cylinder sinusoidally near detuning parameter $\xi\approx0$, we found standing waves rather than the traveling rolls [see Fig. 4(b)], as predicted by theory. Figure 5 shows a phase diagram of the primary transitions from the base flow to standing waves and the secondary transition from standing waves to traveling waves for $\xi\approx0$ as we varied the modulation amplitude R_m and inner cylinder Reynolds number R_i. One interesting feature to note in Fig. 5 is that, when the modulation amplitude is increased above a critical value ($R_m/R_i>0.05$), the standing waves can be excited at R_i values much lower than the critical R_i. Another interesting feature is that as the amplitude of modulation increases, we observe standing waves over a widening range of R_i. The traveling-wave state reappears when R_i increases, as has been observed in other systems [13] and in agreement with the theory [11]. At small modulation amplitudes ($R_m/R_i<0.05$) only the traveling roll state appears when R_i is increased, also in agreement with the theoretical predictions (cf. Fig. 1).

The space-time diagram of the standing waves for $R_m/R_{ic}=0.30$, $R_i=241$, and $\xi=0\pm0.01$ is shown in Fig. 6. During one modulation period the light intensity at a given axial position varies periodically, indicating the presence of standing-wave patterns. The frequency of the standing waves is half the modulation frequency.

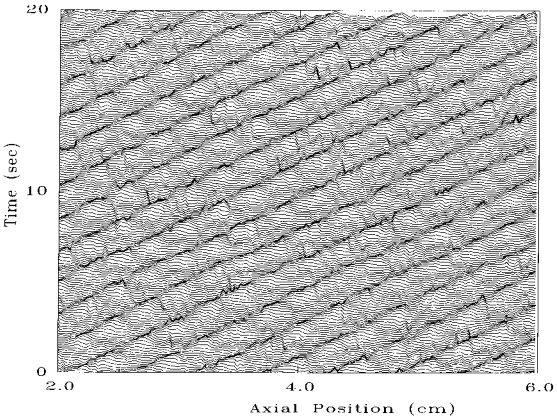

FIG. 8. Space-time diagram of the traveling-wave state at $R_m/R_{ic}=0.212$, $\xi=0.0$, and $R_i=269$ just above the onset (Taylor-Dean system).

A quantitative analysis of the patterns was carried out using two-dimensional Fourier transforms of the patterns in time and space. This proved to be a very useful method for decomposing the standing-wave patterns into their left- and right-traveling wave components from the original space-time CCD data. From the decomposition we obtained the spatial wavelengths, temporal frequencies, and the amplitudes of each component. Figures 7(a) and 7(b) show the right- and left-traveling waves obtained from the space-time data shown in Fig. 6. The power spectra obtained using the two-dimensional fast Fourier transform (FFT) for both right- and left-traveling waves are shown in Figs. 7(c) and 7(d). The left and right components have similar space and time characteristics. The small differences in amplitudes of the spectral peaks may be attributed to slightly nonuniform lighting conditions.

At a still higher inner cylinder speed the standing waves lose their stability to a traveling-wave state. This transition is supercritical within our experimental resolution. No mixed states of standing and traveling rolls have been seen. The space-time diagram for the traveling-wave state just above the onset at $R_i=269$, $R_m/R_{ic}=0.212$ is shown in Fig. 8. The decomposition of this space-time data and associated power spectra are shown in Figs. 9(a)–9(d). These figures show that one traveling mode dominates over the other, much weaker, components present in the system.

We also tested the sensitivity of the onset of the patterns, and which pattern appears first, to variation of the detuning parameter ξ in this system. The result for $R_m/R_i=0.3$, shown in Fig. 10, indicates that the onset of the patterns is very sensitive to the value of the detuning parameter ξ for this system. When $\xi\approx0$ the standing-wave pattern appears at R_i well below $R_{ic}=263$. As we changed ξ away from $\xi=0$ (lower or higher modulation frequencies than $2f_h$) the onset of the patterns was delayed considerably. In fact, at higher modulation frequencies ($\xi<-0.2$) patterns appeared only at *supercritical* R_i ($>R_{ic}$) values for $R_m/R_{ic}=0.3$. Figure 10 also shows that, for fixed R_m, as we move away from $\xi=0$ the characteristics of the patterns also change, so that traveling-wave patterns appear at onset ($\xi<-0.08$ or $\xi>0.04$ for $R_m/R_{ic}=0.3$) rather than standing waves. It is

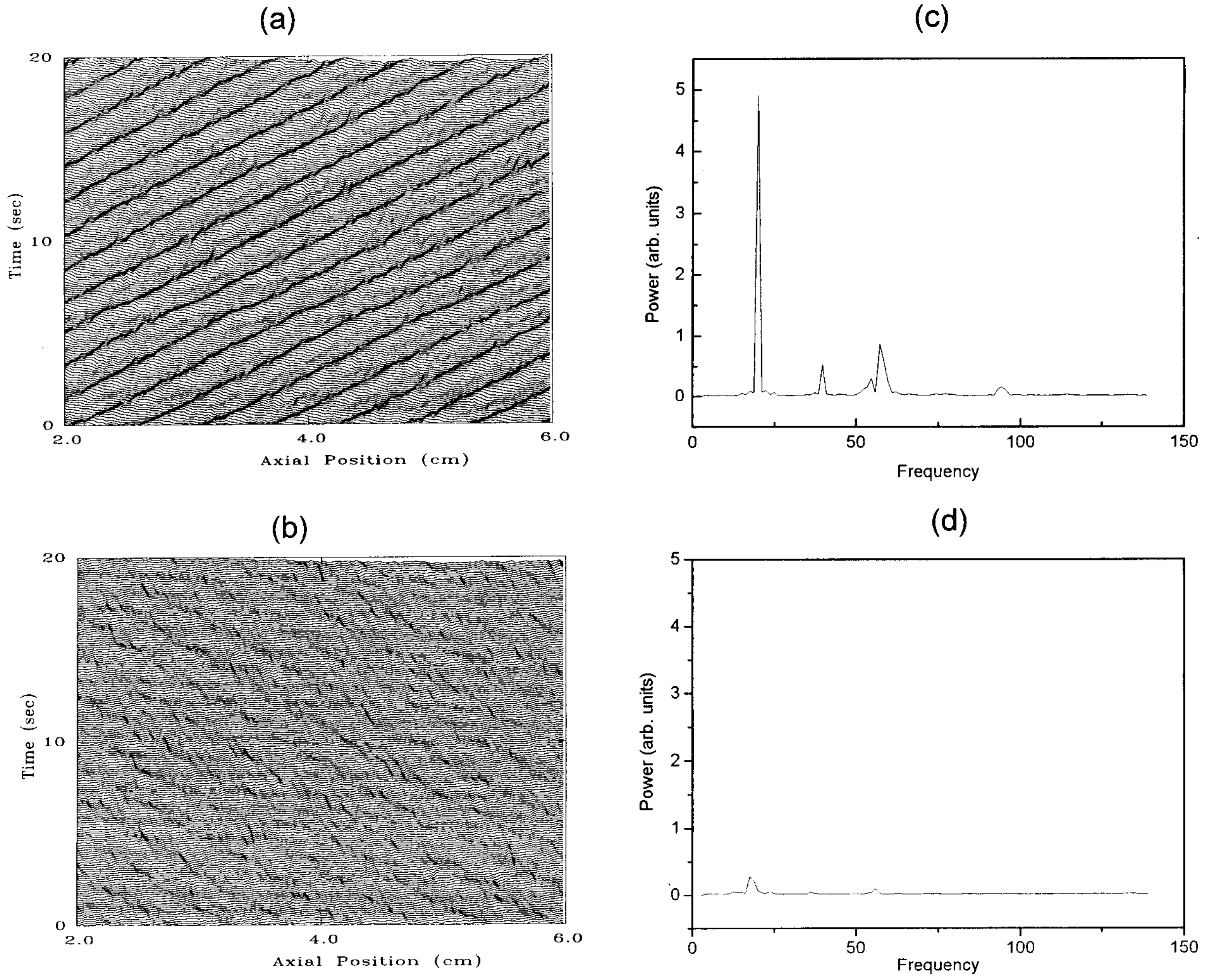

FIG. 9. Space-time diagrams of (a) the right-traveling-wave component and (b) the left-traveling-wave component of the traveling-wave state shown in Fig. 8. (c) and (d) are the frequency power spectra of the decomposed right- and left-traveling modes. The dimensionless frequencies are scaled to the inverse of the diffusive time scale ν/d^2. The right-traveling-wave component dominates the left-traveling component in the system.

possible that even for these large values of $|\xi|$ standing waves would reappear as the critical mode for higher fixed R_m/R_{ic} than 0.3.

Figure 11 shows the ratio of the fractional power under the left (the one induced by the modulation in this case) traveling-wave spectra to the total power, as a function of ξ. This characteristic resonance curve illustrates the disappearance of the left-traveling wave as the detuning parameter ξ shifts away from 0. The maximum fractional power was a little less than the expected 0.5, which can be attributed to the nonideal lighting conditions. We also analyzed the frequencies of the two components as a function of ξ. Figure 12 shows the frequency ratio as a function of ξ. This plot shows the standing-wave region clearly, where the two components lock to the same frequency over a range of ξ. The primary transition to standing waves and the secondary transition to traveling waves in R_m/R_{ic} vs R_i parameter space are very sensitive to ξ for ξ near zero. Figures 13(a) and 13(b) give the phase diagrams when ξ is equal to -0.03 and $+0.03$, which show these phase changes clearly. A comparison of Figs. 13 and 5 shows that the minimal modulation amplitude for the excitation of standing waves is actually lower for

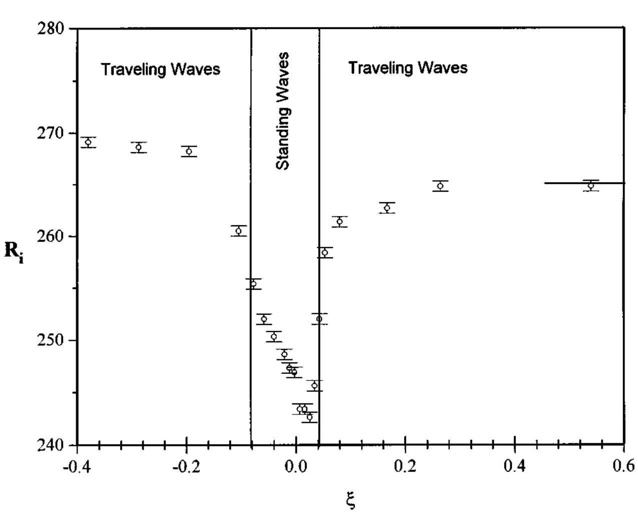

FIG. 10. Onset of the primary flow transition R_i vs the detuning parameter ξ $[=(2f_h-f_m)/2f_h]$ at $R_m/R_{ic}=0.3$ (Taylor-Dean system).

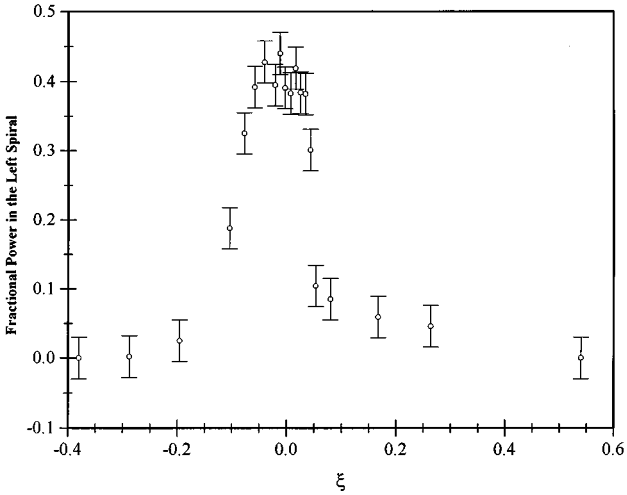

FIG. 11. Fractional power of the secondary traveling-wave state vs the detuning parameter ξ at $R_m/R_{ic}=0.3$.

$\xi=0.03$ than for $\xi=0$. This can be ascribed to the dependence of the linear frequency of the waves on R_i as well as $|b|^2$ and $|w|^2$ as expressed in (8); optimal resonance is obtained for $a_i=0$ rather than $\xi=0$ [cf. (9)].

Further increases in R_i beyond the traveling-wave state resulted in the appearance of short-wavelength modulations near $R_i\simeq300$ and incoherent patterns at $R_i\simeq340$ for $R_m/R_{ic}=0.25$ and $\xi=0$. These patterns and their decomposed left- and right-traveling components are shown in Figs. 14 and 15.

C. Eccentric Taylor-Couette system

In the Taylor-Dean system, the rotational symmetry is strongly broken by the air-liquid interfaces. We now consider a system with slightly broken rotational symmetry, which can be modeled as a perturbation on a system with two translational symmetries (strictly speaking, a pure translation in space along z and a rotational symmetry along ϕ).

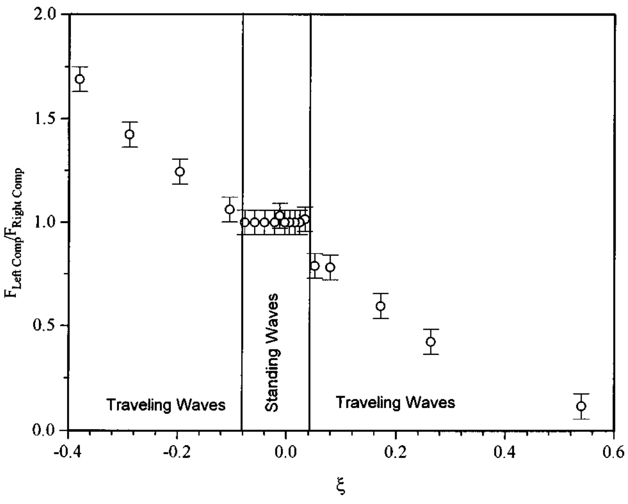

FIG. 12. Frequency ratio of the two traveling-wave components vs the detuning parameter ξ at $R_m/R_{ic}=0.3$. Both left- and right-traveling components have the same frequency within experimental error over a fairly wide region near resonance $\xi=0$.

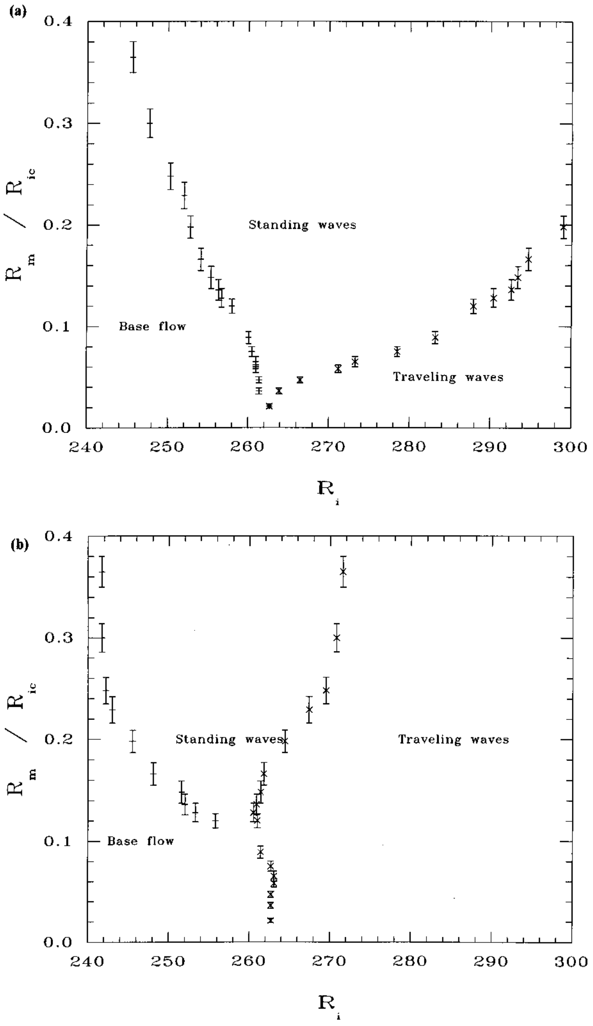

FIG. 13. Phase diagrams when (a) $\xi=-0.03$ and (b) $\xi=0.03$. Pluses and crosses indicate the transitions from the base flow to standing waves and to traveling waves, respectively.

The classical concentric Taylor-Couette system has translational symmetry in the axial direction and rotational symmetry around the axis. As we discussed in Sec. II, for this system it is necessary to apply periodic forcing as well as an azimuthal perturbation to linearly couple the left- and right-traveling spirals to produce the standing waves. We produced an azimuthal perturbation in this system by offsetting the axis of the inner cylinder relative to that of the outer cylinder while maintaining the two axes parallel, thereby making the system eccentric.

The experiment was performed in the region of (R_o, R_i) parameter space where traveling waves in the form of spiral vortices occur as the primary instability. This happens when the cylinders are counterrotating and concentric [16,23–25]. The spiral patterns travel in both the axial and azimuthal directions and break both the axial and azimuthal symmetries of the base flow. For a given radius ratio there is a unique value of outer cylinder speed above which the primary bifurcation from the base flow is a supercritical Hopf bifurcation to the time periodic spiral flow [23,24]. The azimuthal wave

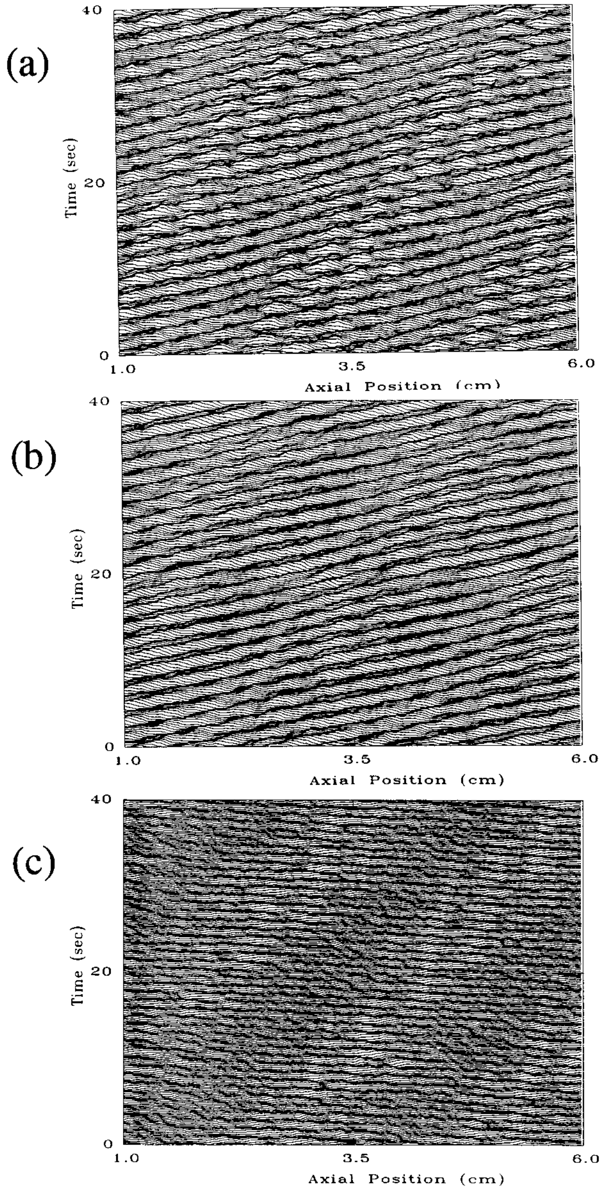

FIG. 14. (a) Traveling-wave state with short-wavelength modulations at $R_i=300$ and $R_m/R_{ic}=0.254$ (Taylor-Dean system). (b) and (c) are the decomposed space-time data for right- and left-traveling modes, respectively, of the same traveling-wave state shown in (a).

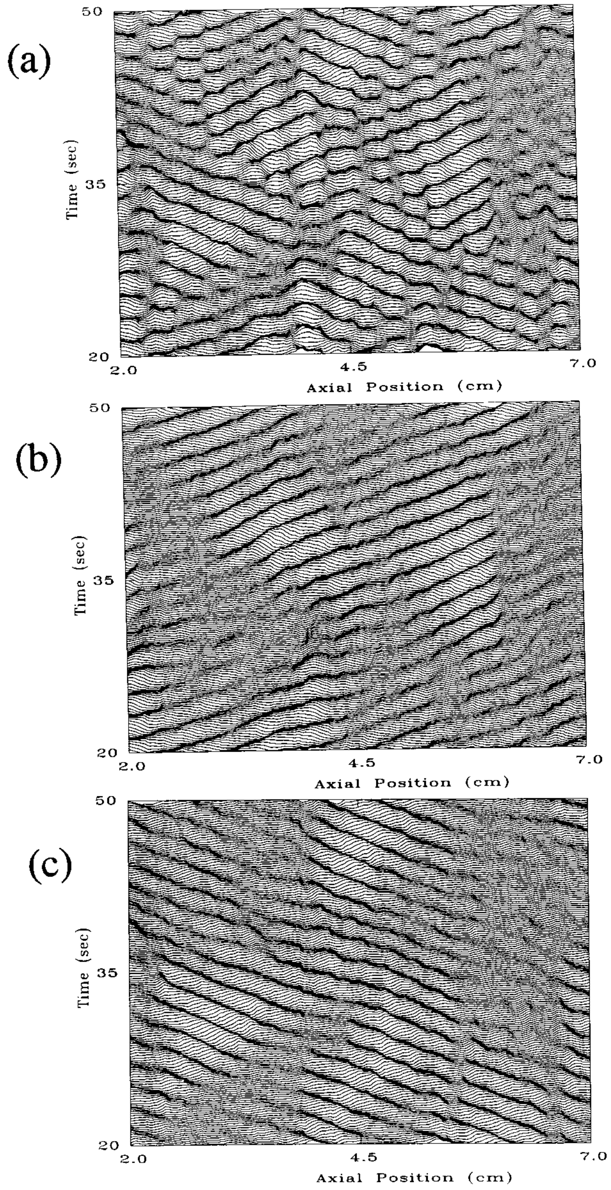

FIG. 15. Incoherent pattern at $R_i=340$ and $R_m/R_{ic}=0.254$ (Taylor-Dean system). (b) and (c) are the decomposed space-time data for right- and left-traveling modes, respectively, of the incoherent pattern shown in (a).

number (m) of the spirals increases as the outer cylinder speed increases. The locations of the crossover points between spirals with different azimuthal wave numbers are uniquely determined by the radius ratio of the two cylinders [24].

Our eccentric Taylor-Couette cylinder system, shown schematically in Fig. 16, consists of an inner cylinder made of black Delrin plastic with radius $r_i=4.76$ cm, an outer cylinder made of Plexiglas with radius $r_o=5.95$ cm, which gives a gap $d=r_o-r_i=1.19$ cm, and a radius ratio $\eta=0.800$. The main control parameters are the inner and outer cylinder Reynolds numbers $R_i=2\pi f_i r_i d/\nu$ and $R_o=2\pi f_o r_o d/\nu$, where d is the average gap width. A stationary support holds the apparatus at the top and the bottom. The outer cylinder is connected to the stationary support by means of bearings at both ends. The upper end of the inner cylinder is attached to a long shaft that hangs from a horizontally movable plate on the stationary framework (see Fig. 16). The lower end of the inner cylinder is left unattached and is suspended approximately 1 mm above the bottom of the system. Eccentricity is adjusted by offsetting the axis of the inner cylinder relative to the fixed axis of the outer cylinder. The position of the axis of the inner cylinder is read to an accuracy of 0.005 cm using a micrometer attached to the stationary support. The eccentricity is $e=\varepsilon/(r_o-r_i)$, where ε is the offset of the two cylinder axes. To maintain consistent end conditions, the upper and lower boundaries of the flow are formed by Teflon rings attached to the outer cylinder and located near the ends of the cylinder. There is a narrow gap of 0.4 cm between

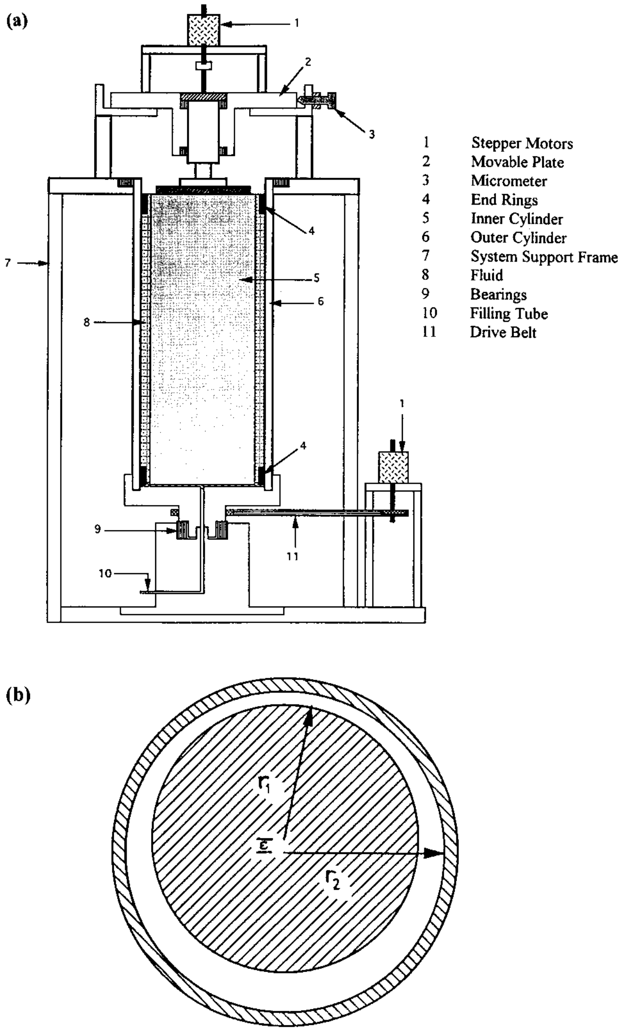

FIG. 16. (a) Vertical and (b) horizontal cross sections of the eccentric cylinders system.

each of these rings and the inner cylinder that is nevertheless wide enough to allow for offsetting the inner cylinder. The length of the fluid column L is 40.40 cm, giving an aspect ratio $\Gamma = L/(r_o - r_i) = 34.0$, large enough to minimize end effects. Again, the working fluid was pure double distilled water or a solution of double distilled water and 44% glycerol by weight with 1% of Kalliroscope AQ1000 added for visualization. The experimentally obtained critical Reynolds number for concentric cylinders when $R_o = 0$ has been compared with reference values to check the accuracy of ν obtained from tabulated data [26]. The difference was less than 1%. Both inner and outer cylinders are driven by two independently rotating Compumotor stepper motors, which are controlled through Compumotor Series 2100 indexers. Since the modulation amplitude required in the eccentric Taylor-Couette system was much greater than for the Taylor-Dean system, we could not use the two motor push rod arrangement to produce both linear and sinusoidal modulation of inner cylinder. Therefore, we have used a single motor to produce both a constant rotation speed component and the sinusoidal modulation of the inner cylinder rotation rate by sending control commands (a sequential change of shaft motion parameters with time delays) to the indexer using the computer. This produces an approximate sinusoidal variation, with more than 40 step changes in velocity per cycle.

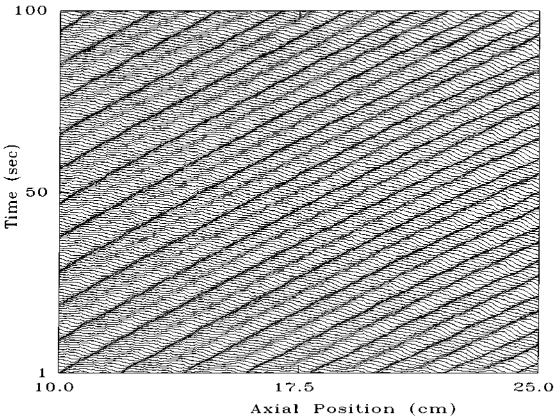

FIG. 17. Space-time diagram of the spiral pattern ($m = 2$) in the Taylor-Couette system at $R_i = 151$, $R_o = 155$, $e = 0$, and $R_m = 0$.

To obtain the location of the onset of patterns for each modulation frequency f_m and modulation amplitude R_m, we employed a method similar to that used in the experiment on the Taylor-Dean system. We kept the outer cylinder speed fixed at a value within the range where the bifurcation to spiral vortices occurs. Then, at a fixed modulation amplitude R_m and constant frequency f_m, we increased the average inner cylinder speed until the pattern appeared. Then several sets of space-time data were taken while increasing R_i. We repeated this procedure with increasing amplitudes R_m and various detuning parameters ξ (i.e., frequencies around twice the Hopf frequency, where the Hopf frequency in this case is the frequency of the spiral pattern near onset in the absence of modulation).

D. Results and discussion

When there is no modulation the base flow bifurcates supercritically to spirals as we increase the inner cylinder speed while keeping the outer cylinder speed constant. A typical space-time diagram for the spiral pattern near onset ($R_i = 151$, $R_o = 155$, and $R_m = 0$) is shown in Fig. 17. Here the intensity of a line parallel with the axis of the cylinders was

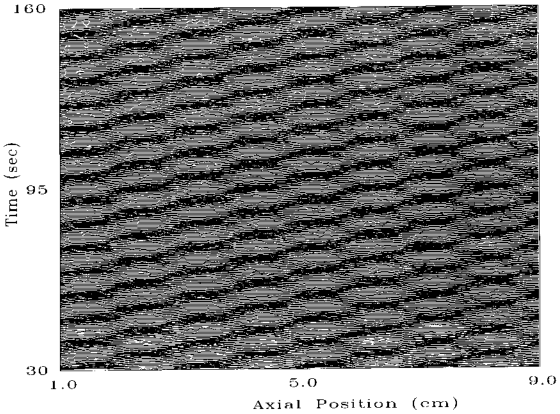

FIG. 18. Space-time diagram of the standing-wave-like pattern in the Taylor-Couette system at $R_i = 151$, $R_o = 155$, $e = 0.126$, $R_m/R_{ic} = 0.4$, and $\xi = 0$.

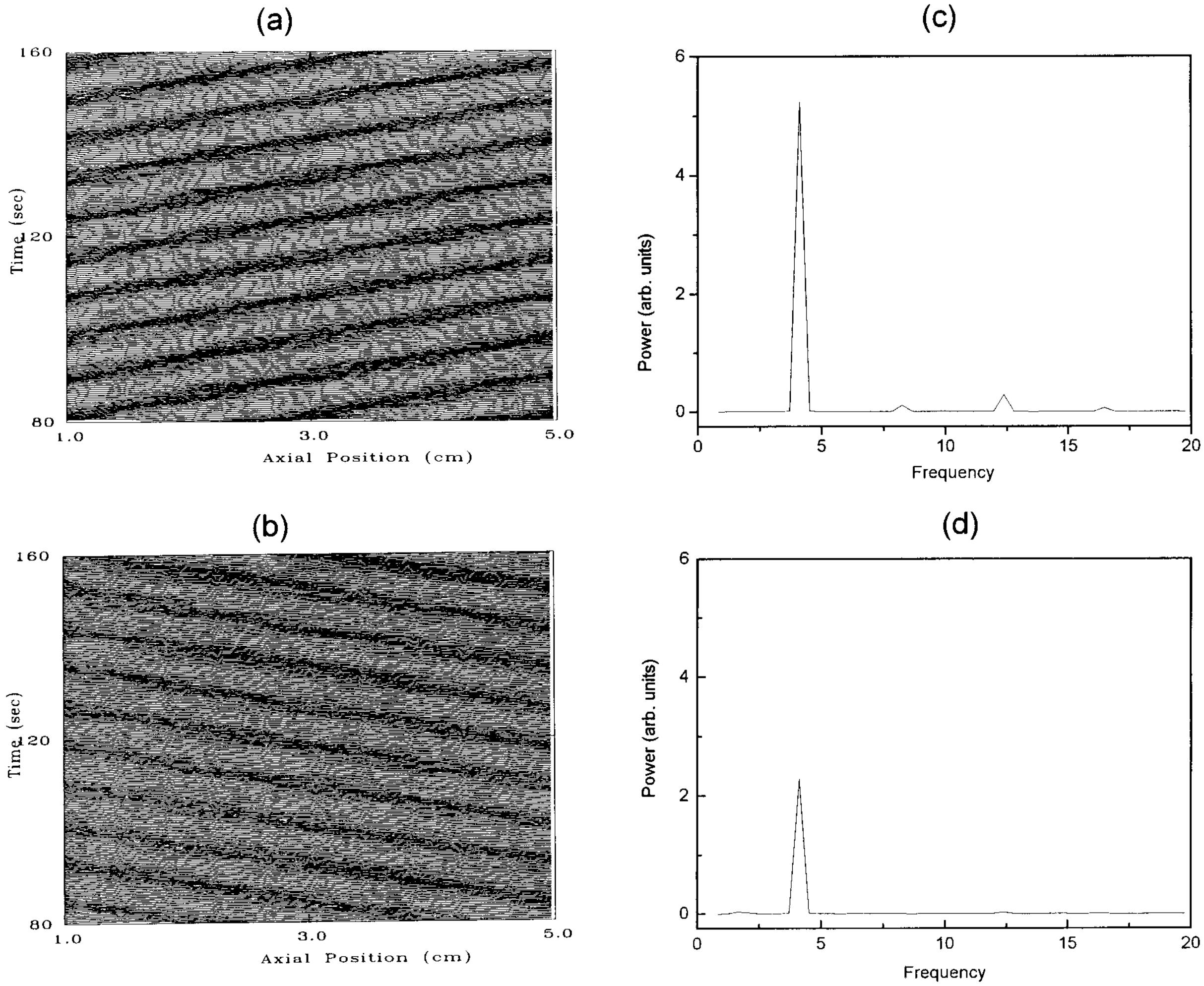

FIG. 19. (a) and (b) are the decomposed components of the space-time data in Fig. 18. (c) and (d) are the frequency power spectra of the right- and left-traveling modes. The frequencies are scaled to the inverse of the diffusive time scale ν/d^2. The right-traveling-wave component dominates the left-traveling component in the system.

recorded every 0.6 sec for 100 sec. The wavelength of the spirals along the axis of the cylinder is $\lambda=2.07$ cm$\approx 2d$. Light sheet visualization through the gap cross section shows that the spirals exist near the inner cylinder. At ϵ $[=(R_i-R_{ic})/R_{ic}]$ slightly greater than zero the pattern fills most of the working space along the axis. An upward-moving spiral exists near the bottom of the system and a downward-moving spiral exists near the top. A horizontal defect line forms where the two spirals meet. These defect lines are not necessarily halfway between the top and the bottom along the axis of the cylinders. Such defects are inherent to traveling-wave patterns [27]. The frequency of the spirals (Hopf frequency) with azimuthal wave number $m=2$, as shown in Fig. 17, near the onset ($R_{ic}=151$, $R_o=155$ for $e=0$) is 0.113 Hz.

When we sinusoidally modulated the inner cylinder rotation speed, we observed wave patterns that resemble standing waves (time-dependent patterns that are stationary in space) rather than traveling waves (spirals) as the first bifurcation from the base flow. Figure 18 shows a space-time diagram of the standing-wave-like pattern near the transition to the spiral state with azimuthal wave number $m=2$ at $R_i=151$, $R_o=155$, $R_m/R_i=0.4$, $e=0.126$, and $\xi\approx 0$. Figures 19(a) and 19(b) show the resulting right- and left-traveling waves obtained from the space-time data shown in Fig. 18. The power spectra obtained using the two-dimensional FFT for right- and left-traveling wave components, shown in Figs. 19(c) and 19(d), have the same frequency characteristics, but different peak amplitudes. A true standing wave would have equal amplitudes in the traveling components. Even at very high modulation amplitudes R_m, one spiral component always dominates the other. Figure 20 shows the ratio of the amplitudes of the primary peaks of the two spiral components versus modulation frequency f_m.

Figure 21 shows the phase diagram of R_m/R_{ic} vs R_i for $e=0.168$ and $\xi\approx 0$. This shows that the base flow became unstable at lower R_i as the amplitude of modulation R_m increased, in agreement with the theoretical predictions. Also, the standing-wave-like patterns appeared only at large modulation amplitudes (for $e=0.168$, $R_m/R_i>0.17$) when the detuning parameter $\xi\approx 0$. At small modulation amplitudes ($R_m/R_i<0.17$) only the traveling roll (spiral) state appears when R_i is increased. Whether standing-wave-like patterns are produced also depends on the eccentricity of the system. For small eccentricity e, they appeared only at higher modulation amplitudes, in agreement with the theoretical predictions.

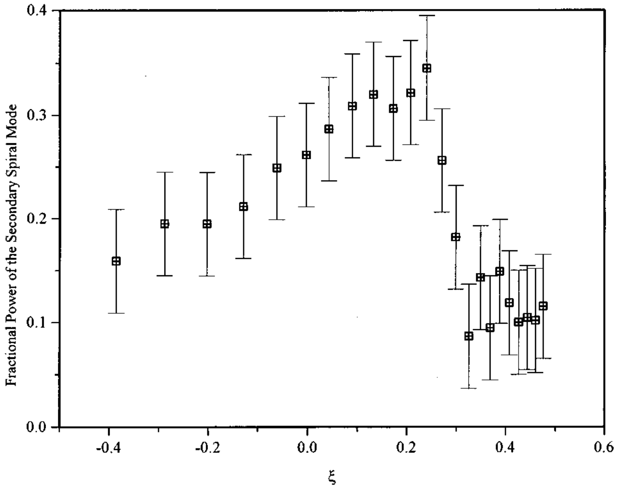

FIG. 20. Ratio of the spectral peak amplitude of the secondary spiral wave state to the spectral peak amplitude of the primary spiral wave state vs the detuning parameter ξ at $R_i=151$, $R_o=155$, $R_m/R_{ic}=0.53$, and $e=0.126$.

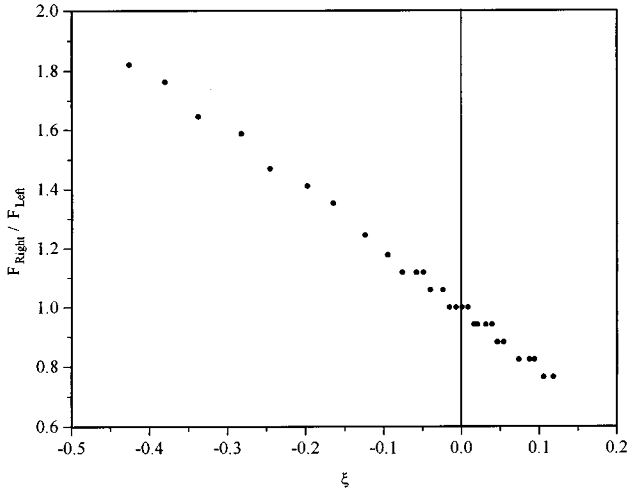

FIG. 22. Frequency ratio of the two traveling-wave components versus the detuning parameter ξ in the eccentric Taylor-Couette system at $R_i=151$, $R_o=155$, $R_m/R_{ic}=0.53$, and $e=0.126$. The left- and right-traveling components have the same frequency, only in a very small region near resonance $\xi=0$.

Compared with other systems (e.g., the Taylor-Dean system discussed in Sec. III B or electroconvection of nematic liquid crystals and binary fluid convection [13]), in this system, the standing-wave-like patterns with two components having the same frequency appear only in a small region of parameter space near the resonance frequency (see Fig. 22). Both the small region of parameter space and the unequal power spectra amplitudes indicate that the coupling of the modulation to the fluid flow is very weak. Two factors may contribute to this. Equations (5) and (6) show that the azimuthal symmetry breaking employed in the experiment ($n=1$) enters the coupling between left- and right-traveling spirals only with its fourth power for spirals with $m=2$. Thus quite large eccentricities are needed to give a strong effect. Motivated by this observation, we have also studied the modulation of $m=1$ spirals. However, no resonant excitation of standing waves was observed; instead, the patterns relax to the base flow during part of the cycle. Since the frequency of the waves is very small, they appear to follow the periodic forcing adiabatically, indicating that their growth rate is of the same order as the forcing frequency. Therefore, for (5) and (6) to apply, the growth rate would have to be reduced substantially. This would require much higher resolution in the average Reynolds numbers than is accessible in the present apparatus. The investigation of $m=1$ spirals is further complicated by the presence of other modes such as axisymmetric vortices and interpenetrating spirals at nearby parameter values.

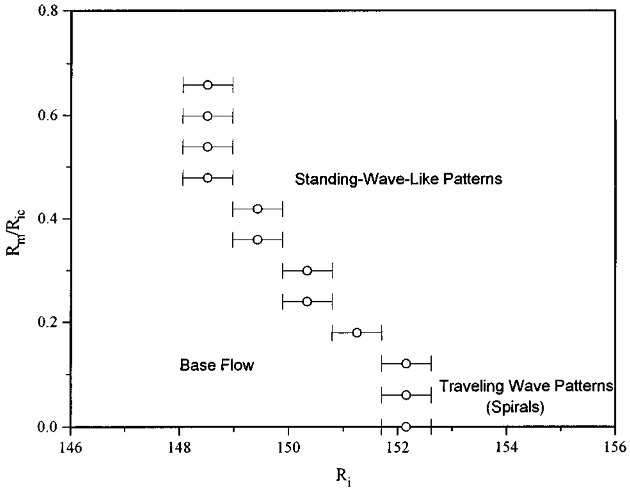

FIG. 21. Phase diagram of R_m/R_{ic} versus R_i for the eccentric Taylor-Couette system with eccentricity $e=0.168$ and detuning parameter $\xi=0$.

A second reason for the apparent weakness of the coupling is presumably the penetration depth of the oscillation into the bulk of the fluid, as characterized by the viscous Stokes layer of width $\delta=\sqrt{\nu/\omega}$, near the inner cylinder. The thickness of the Stokes layer δ at $\xi=0$ for both $m=1$ and 2 spiral states are 0.24 and 0.17 cm, much smaller than the size of the gap $d=1.19$ cm. Thus the bulk of the fluid feels the modulation only very weakly. (It is possible that similar effects may have been present in the binary fluid convection experiment reported in [13]. This may have contributed to the less well-defined standing waves reported there, in contrast with the electroconvection experiments.) Furthermore, in the eccentric Taylor-Couette system, modulation creates only a weak azimuthal pressure gradient due to the small eccentricity and the oscillatory Stokes layer influence may not be enough to excite a strong secondary traveling component. In the Taylor-Dean system, on the other hand, the inner cylinder modulation creates not only the oscillatory boundary layer influence but also an induced oscillatory azimuthal pressure gradient across the whole gap, due to the free surface, which more readily affects the pattern.

The standing-wave-like patterns appearing in the eccentric Taylor-Couette system for $\xi=0$ near the transition boundary to the $m=2$ spiral state lose their stability to an incoherent pattern when the inner cylinder speed is increased further above the onset. This may be due to the loss of stability of the basic spirals to interpenetrating spirals and wavy spirals. Even for the concentric cylinder case ($e=0$) we have seen some evidence of a weak secondary spiral at very high modulation amplitudes. This could be due to small imperfections in the experimental apparatus (e.g., nonparallel cylinder axes), which may break the rotational symmetry sufficiently to induce a second spiral.

IV. CONCLUSION

In conclusion, we have found that time-periodic modulation at close to twice the frequency of a Hopf bifurcation can induce standing waves in systems with traveling-wave patterns in two directions. The Taylor-Couette system with counterrotating cylinders produces spirals at onset over a large parameter range, but unless the rotational symmetry of the apparatus is broken, standing waves cannot be excited by modulation. This is in contrast with the case of one-dimensional traveling-wave patterns studied in convection [13], where only temporal modulation is necessary to excite standing-wave patterns. Temporal modulation of the eccentric Taylor-Couette system induces a second traveling spiral pattern as predicted by theory. However, owing partly to weak coupling of the oscillations to the bulk of the flow, it never grows to a large enough amplitude, nor does it couple with the other traveling spiral sufficiently strongly, to produce simple standing-wave patterns at onset. The temporally modulated Taylor-Dean system, in contrast, with its strongly broken azimuthal symmetry, yields clear agreement with the qualitative features of the theoretical model.

ACKNOWLEDGMENTS

C.D.A., S.G.K.T., and J.J.H. thank ONR for support through Grants Nos. N00014-86-K-0071 and N00014-89-J-1352. H.R. gratefully acknowledges discussions with J. D. Crawford and E. Knobloch. His work was supported by DOE through Grant No. DE-FG02-92ER14303.

[1] S. H. Davis, Annu. Rev. Fluid Mech. **8**, 57 (1976), and references therein.
[2] J. J. Niemela and R. J. Donnelly, Phys. Rev. Lett. **59**, 2431 (1987).
[3] G. Seminara and P. Hall, Proc. R. Soc. London Ser. A **350**, 299 (1976).
[4] R. J. Donnelly, Proc. R. Soc. London Ser. A **281**, 130 (1964).
[5] G. Ahlers, P. C. Hohenberg, and M. Lücke, Phys. Rev. A **32**, 3493 (1985).
[6] T. J. Walsh and R. J. Donnelly, Phys. Rev. Lett. **58**, 2543 (1988).
[7] P. Hall, J. Fluid Mech. **67**, 29 (1975).
[8] P. J. Riely and R. L. Laurence, J. Fluid Mech. **75**, 625 (1976).
[9] C. F. Barenghi and C. A. Jones, J. Fluid Mech. **208**, 127 (1989).
[10] S. Carmi and J. I. Tustaniwskyj, J. Fluid Mech. **108**, 19 (1981).
[11] H. Riecke, J. D. Crawford, and E. Knobloch, Phys. Rev. Lett. **61**, 1942 (1988).
[12] D. Walgraef, Europhys. Lett. **7**, 485 (1988).
[13] I. Rehberg, S. Rasenat, J. Fineberg, M. de la Torre Juarez, and V. Steinberg, Phys. Rev. Lett. **61**, 2449 (1988).
[14] M. C. Cross and P. C. Hohenberg, Rev. Mod. Phys. **65**, 851 (1993).
[15] H. Riecke, Europhys. Lett. **11**, 213 (1990).
[16] C. D. Andereck, S. S. Liu, and H. L. Swinney, J. Fluid Mech. **164**, 155 (1986).
[17] Y. Demay and G. Iooss, J. Méc. Théor. Appliq. special issue, 193 (1984).
[18] I. Mutabazi, J. J. Hegseth, C. D. Andereck, and J. E. Wesfreid, Phys. Rev. Lett. A **64**, 1729 (1990).
[19] I. Mutabazi, J. J. Hegseth, C. D. Andereck, and J. E. Wesfreid, Phys. Rev. A **38**, 4752 (1988).
[20] D. B. Brewster and A. H. Nissan, Chem. Eng. Sci. **7**, 215 (1958).
[21] I. Mutabazi, C. Normand, H. Peerhossaini, and J. E. Wesfreid, Phys. Rev. A **39**, 763 (1988).
[22] J. Hegseth, Ph.D. dissertation, The Ohio State University, 1990 (unpublished).
[23] W. F. Langford, R. Tagg, E. Kostelich, H. L. Swinney, and M. Golubitsky, Phys. Fluids **31**, 776 (1988).
[24] R. Tagg, W. S. Edwards, and H. L. Swinney, Phys. Rev. A **39**, 3734 (1989).
[25] S. G. K. Tennakoon and C. D. Andereck, Phys. Rev. Lett. **71**, 3111 (1993).
[26] *CRC Handbook of Chemistry and Physics*, edited by D. R. Lide (CRC, Boca Raton, FL, 1991), p. D-192.
[27] L. Gil and J. Lega, in *Propagation in Systems Far from Equilibrium*, edited by J. E. Wesfreid, H. R. Brand, P. Manneville, G. Albinet, and N. Boccara (Springer-Verlag, New York, 1987), p. 164.